Journal of Sound and Vibration (1997) **204**(3), 477–494

ANISOTROPY AND STRUCTURAL COUPLING ON VIBRATION AND INSTABILITY OF SPINNING THIN-WALLED BEAMS†

O. SONG

Mechanical Engineering Department, Choong-Nam National University, Taejon, 305–764, Korea

AND

L. LIBRESCU

Engineering Science and Mechanics Department, Virginia Polytechnic Institute and State University, Blacksburg, VA, 24061, U.S.A.

(*Received* 4 *October* 1996, *and in final form* 31 *December* 1996)

The problem of the mathematical modelling of anisotropic beams rotating with constant angular speed about their longitudinal body-axis fixed in the inertial space is addressed. The analysis is conducted in the context of a refined theory of thin-walled anisotropic composite beams which incorporates a number of non-classical effects. Among them, there are the transverse shear, the primary and secondary warping effects. Special attention is paid to the influence played by anisotropy of constituent materials, boundary conditions and spinning speed on forward and backward precession frequencies and on instability speed. A number of applications involving both axisymmetric and doubly symmetric cross-section beams are presented and pertinent conclusions are outlined.

1. INTRODUCTION

A growing interest toward the incorporation of composite material systems in the design of rotating structures (e.g., turbine and helicopter blades, tilt rotor aircraft, rotating shafts and robotic manipulator arms) has been manifested in the last few years.

This trend, which is likely to continue and intensify, is driven by the demands of lighter and more flexible structures, capable of higher performance, as compared to their metallic counterparts. By virtue of their directionality property, the composite material systems provide unique capabilities enabling one to achieve totally new types of elastic couplings. Such a design, leading for example to the coupling between bending and torsional behavior of a beam has been successfully employed in the design of the X-29 swept-forward wing aircraft in order to eliminate, without weight penalties, the aeroelastic divergence instability. Another type of coupling, between extension and twist, is of interest for applications in helicopter and turbine blades and in tilt-rotor aircraft.

A class of rotating structures, namely the one characterized by the angular velocity vector (spin rate vector) parallel to their longitudinal axis, plays a great role in the advanced technology (see references [1–3]). This type of structures is found in gas turbines

† This paper represents an amended version of that presented at the 37th AIAA/ASME/ASCE/AHS/ASC Structures, Structural Dynamic and Materials Conference April 1996 Salt Lake City, UT.

0022–460X/97/280477 + 18 $25.00/0/sv960947

for higher power aircraft engines, in helicopter drive applications, in space structures such as satellite booms as well as in modern machinery.

The incorporation of the new composite materials for future high performance spinning structural systems constitutes a natural trend which is likely to grow in the years ahead. However, in order to exploit in the best way the capabilities provided by the new material systems, a better understanding of the implications on the dynamic response characteristics of elastic couplings generated by their anisotropy is needed. The clarification of this problem constitutes one of the basic goals of this paper. In addition, it aims to supply a comprehensive derivation and solution of the dynamics of spinning structures modelled as thin-walled beams under various boundary conditions. Due to the complexity of accelerations acting throughout the system, the analysis of spinning structures differs from that of their non-rotating counterparts. Indeed, in addition to the accelerations arising from elastic structural deformations, the ones associated with Coriolis and centripetal effects have to be included into the system.

The derived governing equations incorporate a number of non-classical effects such as transverse shear, warping inhibition, rotatory inertia, Coriolis acceleration and anisotropy of the spinning structure.

Although the pertinent governing equations are obtained for the case of an arbitrary cross-section, the numerical applications are confined to the case of a rectangular cross-sectional beam.

Based on these equations, the problem of the frequency spectrum corresponding to the backward and forward precession, as well as the determination of the critical spin rates (i.e., of such spin rates for which the structure frequencies go to zero, this resulting in a divergence-type instability) are investigated.

In order to achieve an increase of the spin rate without the occurrence of instability by divergence (i.e., in order to optimize the spinning structure), a structural tailoring analysis is pursued. To this end, a *circumferentially uniform stiffness configuration* is implemented, in which context the entire system of governing equations splits exactly into two independent systems, one of them involving the bending–bending–transverse shear couplings and the other one involving the twist–extension coupling (see references [4, 5]).

The available body of literature reveals that this problem was approached in the framework of the solid beam theory (i.e., within the Euler–Bernoulli [1, 6–10] and Timoshenko [11–14] beam models), and of circular cylindrical shell theory [15–19]. Moreover, with a few exceptions, the analysis was generally done in the context of metallic structures only.

To the best of the authors' knowledge, this study presents for the first time a comprehensive modelling and analysis of advanced spinning structures modelled as thin walled anisotropic beams in which, towards the goal of optimizing their dynamic performances, the tailoring technique is implemented.

2. CO-ORDINATE SYSTEMS AND BASIC ASSUMPTIONS

The case of a straight untwisted flexible beam of length L spinning along its longitudinal z-axis at a constant rate Ω is considered (see Figure 1). Two sets of co-ordinates, an inertial one $OXYZ$, and a rotating frame of reference $Oxyz$ with the common origin O, located in the geometric center (coinciding with the elastic center of the beam), are considered. It is supposed that at $t = 0$, the axes of the two systems coincide while, in the undeformed configuration, the body-fixed and inertial co-ordinates Oz and OZ coincide at any time t. Associated with the co-ordinate systems (x, y, z) and (X, Y, Z) one defines the unit vectors $(\mathbf{i}, \mathbf{j}, \mathbf{k})$ and $(\mathbf{I}, \mathbf{J}, \mathbf{K})$, respectively. In addition to the previously defined system

co-ordinates, a local (surface) one, (n, s, z) associated with the beam is considered. In the light of the stipulated assumptions one can represent the spin rate vector $\mathbf{\Omega}$ as $\mathbf{\Omega} = \Omega\mathbf{k}(\equiv\Omega\mathbf{K})$ with $\dot{\mathbf{\Omega}} = 0$.

The adopted structural model is that of a thin-walled beam. In this context, the case of a single-cell thin-walled beam of arbitrary cross-sectional shape is considered. Toward its modelling the following assumptions are adopted: (1) the original cross-section of the beam is preserved, (2) both primary and secondary warping effects are included, (3) transverse shear effects are incorporated and finally, (4) the constituent material of the structure features anisotropic properties, and, in this context, a special layup inducing flapping–lagging coupling is implemented.

3. KINEMATICS

In light of the previously mentioned assumptions and in order to reduce the 3-D elasticity problem to an equivalent 1-D one, the components of the displacement vector are represented as (see e.g., reference [5])

$$u(x, y, z; t) = u_0(z; t) - y\phi(z; t), \qquad v(x, y, z; t) = v_0(z; t) + x\phi(z; t),$$

$$w(x, y, z; t) = w_0(z; t) + \theta_x(z; t)[y(s) - n\,\mathrm{d}x/\mathrm{d}s] + \theta_y(z; t)[x(s) + n\,\mathrm{d}y/\mathrm{d}s] - \phi'(z; t)[F_\omega(s) + na(s)]. \tag{1a–c}$$

In these equations $u_0(z; t)$, $v_0(z; t)$, $w_0(z; t)$ denote the rigid body translations along the x-, y- and z-axes while $\phi(z; t)$ and $\theta_x(z; t)$, $\theta_y(z, t)$ denote the twist about the z-axis and rotations about the x- and y-axes, respectively. The expressions of θ_x and θ_y as well as of the geometric quantity $a(s)$ are (see reference [5])

$$\theta_x(z; t) = \gamma_{yz}(z; t) - v_0'(z; t), \qquad \theta_y(z; t) = \gamma_{xz}(z; t) - u_0'(z; t),$$

$$a(s) = -y(s)\,\mathrm{d}y/\mathrm{d}s - x(s)\,\mathrm{d}x/\mathrm{d}s. \tag{2a–c}$$

In equations (1), $F_\omega(s)$ and $na(s)$ play the role of primary and secondary warping functions, respectively. For their definition see e.g., references [5, 20].

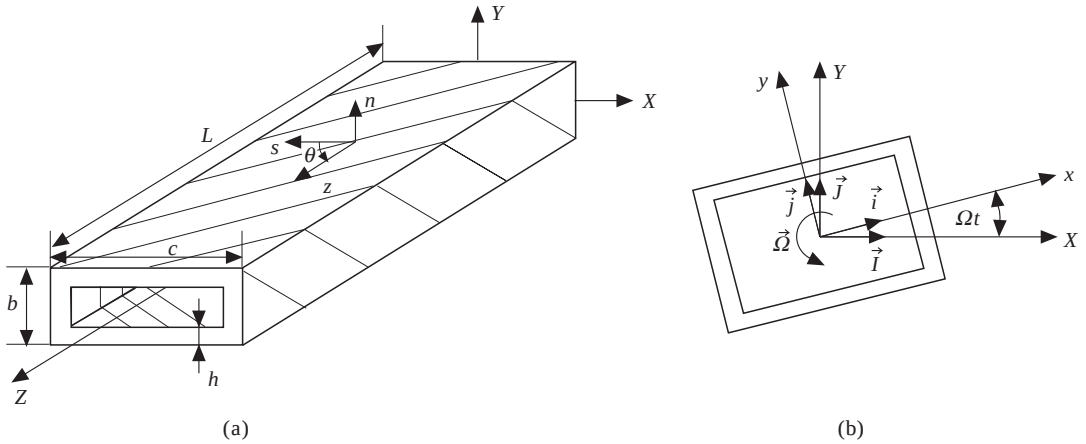

Figure 1. (a) Thin-walled beam featuring CUS configuration, (b) cross-section of the beam.

It is readily seen that by virtue of equations (1) and (2), the statement of the cross-section non-deformability (implying $\epsilon_{xx} = 0$; $\epsilon_{yy} = 0$ and $\gamma_{xy} = 0$ and, consequently, $\epsilon_{nn} = \epsilon_{ss} = \gamma_{sn} = 0$), as well as the continuity requirement of w along the mid-line contour (i.e., $\oint (\partial w/\partial s)\, \mathrm{d}s = 0$) are fulfilled. It is also seen that in the absence of transverse shear effects

$$\theta_x(z; t) = -v_0'(z; t), \qquad \theta_y(z; t) = -u_0'(z, t). \tag{3}$$

In these equations, as well as in the forthcoming ones, the primes denote differentiation with respect to the longitudinal z-co-ordinate. The position vector of a point $M(x, y, z)$ belonging to the deformed structure is

$$\mathbf{R}(x, y, z; t) = (x + u)\mathbf{i} + (y + v)\mathbf{j} + (z + w)\mathbf{k}, \tag{4}$$

where x, y and z are the Cartesian co-ordinates of the points of the continuum in its undeformed state. Recalling that the spin rate was assumed to be constant, the velocity and acceleration of point M are

$$\dot{\mathbf{R}} = [\dot{u} - \Omega(y + v)]\mathbf{i} + [\dot{v} + \Omega(x + u)]\mathbf{j} + \dot{w}\mathbf{k},$$

$$\ddot{\mathbf{R}} = [\ddot{u} - 2\Omega\dot{v} - (x + u)\Omega^2]\mathbf{i} + [\ddot{v} + 2\Omega\dot{u} - (y + v)\Omega^2]\mathbf{j} + \ddot{w}\mathbf{k}. \tag{5a, b}$$

In these equations the superposed dots denote derivatives with respect to the time t.

4. GOVERNING EQUATIONS

Toward the goal of deriving the equations of motion of spinning beams, and the associated boundary conditions, Hamilton's variational principle is used. This variational principle may be stated as

$$\delta J = \int_{t_0}^{t_1} \left[\int_\tau \sigma_{ij}\delta\epsilon_{ij}\, \mathrm{d}\tau - \delta K - \int_{\Omega_\sigma} s_i \delta v_i\, \mathrm{d}\Omega - \int_\tau \rho H_i \delta v_i\, \mathrm{d}\tau \right] \mathrm{d}t = 0, \tag{6}$$

where

$$U = \frac{1}{2}\int_\tau \sigma_{ij}\epsilon_{ij}\, \mathrm{d}\tau \qquad \text{and} \qquad K = \frac{1}{2}\int_\tau \rho(\dot{\mathbf{R}} \cdot \dot{\mathbf{R}})\, \mathrm{d}\tau \tag{7a, b}$$

denotes the strain energy functional and the kinetic energy, respectively.

In these equations, t_0 and t_1 denote two arbitrary instants of time; $\mathrm{d}\tau (\equiv \mathrm{d}n\, \mathrm{d}s\, \mathrm{d}z)$ denotes the differential volume element; $\mathbf{s}_i (\equiv \underset{\sim}{\sigma}_{ij} n_j)$ denote the prescribed components of the stress vector on a surface element of the undeformed body characterized by the outward normal components n_i; H_i denote the components of the body forces; Ω_σ denotes the external area of the body over which the stresses are prescribed; ρ denotes the mass density; an undertilde sign identifies a prescribed quantity while δ denotes the variation sign. In equations (6) and (7) the Einstein summation convention applies to repeated indices where Latin indices range from 1 to 3. In the same equations, $(v_1, v_2, v_3) \equiv (u, v, w)$, $(x_1, x_2, x_3) \equiv (x, y, z)$.

In light of equations (1), (4), (5) and (7) and knowing that $\delta v_i = 0$ at t_0, t_1, it can readily be shown that

$$\int_{t_0}^{t} \delta K \, \mathrm{d}t \left(\equiv - \int_{t_0}^{t_1} \mathrm{d}t \int_{\tau} \rho \ddot{\mathbf{R}} \cdot \delta \mathbf{R} \, \mathrm{d}\tau \right)$$

$$= - \int_{t_0}^{t_1} \mathrm{d}t \int_{\tau} \{[\ddot{u} - 2\Omega\dot{v} - \Omega^2(x+u)]\delta u + [\ddot{v} + 2\Omega\dot{u} - (y+v)\Omega^2]\delta v + \ddot{w}\delta w]\rho \, \mathrm{d}\tau$$

$$= - \int_{t_0}^{t_1} \mathrm{d}t \int_{\tau} [[\ddot{u}_0 - y\ddot{\phi} - 2\Omega(\dot{v}_0 + x\dot{\phi}) - \Omega^2(x + u_0 - y\phi)](\delta u_0$$

$$+ y\delta\phi) + [\ddot{v}_0 + x\ddot{\phi} + 2\Omega(\dot{u}_0 - y\dot{\phi}) - (y + v_0 + x\phi)\Omega^2](\delta v_0 + x\delta\phi)$$

$$+ [\ddot{w}_0 + (y - n\,\mathrm{d}x/\mathrm{d}s)\ddot{\theta}_x + (x + n\,\mathrm{d}y/\mathrm{d}s)\ddot{\theta}_y - \ddot{\phi}'(F_w + na)]\delta[w_0 + \theta_x(y - n\,\mathrm{d}x/\mathrm{d}s)$$

$$+ \theta_y(x + n\,\mathrm{d}y/\mathrm{d}s) - \phi'(F_\omega + na)\}) \, \rho \mathrm{d}\tau.$$

In order to induce the elastic coupling between flapwise bending and chordwise bending, a special ply angle distribution referred to as *circumferentially uniform stiffness* (CUS) configuration (see references [4] and [21]) achieved by skewing angle plies with respect to the beam axis according to the law $\theta(y) = \theta(-y)$, is implemented. Angle θ denotes the dominant ply orientation in the upper and lower surface wall configurations. In this case, based on equations (7) and (8) and on constitutive equations displayed in references [5] and [20], from the variational principle (equation (6)), the equations of motion and the boundary conditions involving this type of coupling are obtained. Employment of constitutive equations and strain-displacement relationships in these equations results in the following *governing equations*:

$$\begin{aligned}
\delta u_0: &\quad a_{43}\theta_x'' + a_{44}(u_0'' + \theta_y') = b_1\ddot{u}_0 - \underline{2b_1\Omega\dot{v}_0} - b_1u_0\Omega^2,\\
\delta v_0: &\quad a_{52}\theta_y'' + a_{55}(v_0'' + \theta_x') = b_1\ddot{v}_0 + \underline{2b_1\Omega\dot{u}_0} - b_1v_0\Omega^2,\\
\delta\theta_y: &\quad a_{22}\theta_y'' + a_{25}(v_0'' + \theta_x') - a_{44}(u_0' + \theta_y) - a_{43}\theta_x' = (b_5 + b_{15})\ddot{\theta}_y,\\
\delta\theta_x: &\quad a_{33}\theta_x'' + a_{34}(u_0'' + \theta_y') - a_{55}(v_0' + \theta_x) - a_{52}\theta_y' = (b_4 + b_{14})\ddot{\theta}_x,
\end{aligned} \tag{9a–d}$$

and the *boundary conditions* at $z = 0, L$:

$$\begin{aligned}
\delta u_0: &\quad Q_x = \underset{\sim}{\mathbf{Q}}_x \quad \text{or} \quad u_0 = \underset{\sim}{\mathbf{u}}_0; \qquad \delta v_0: \quad Q_y = \underset{\sim}{\mathbf{Q}}_y \quad \text{or} \quad v_0 = \underset{\sim}{\mathbf{v}}_0;\\
\delta\theta_y: &\quad M_y = \underset{\sim}{\mathbf{M}}_y \quad \text{or} \quad \theta_y = \underset{\sim}{\boldsymbol{\theta}}_y; \qquad \delta\theta_x: \quad M_x = \underset{\sim}{\mathbf{M}}_x \quad \text{or} \quad \theta_x = \underset{\sim}{\boldsymbol{\theta}}_x.
\end{aligned} \tag{10a–d}$$

Herein $Q_x(z;t)$ and $Q_y(z;t)$ denote the shear forces in the x and y directions, while $M_x(z;t)$ and $M_y(z;t)$ denote the moments about the x- and y-axis, respectively. Their definitions can be found in references [5] and [20]. In terms of displacement quantities the static version of homogeneous boundary conditions reads:

$$\begin{aligned}
\delta u_0: &\quad a_{43}\theta_x' + a_{44}(u_0' + \theta_y) = 0; \qquad \delta v_0: \quad a_{52}\theta_y' + a_{55}(v_0' + \theta_x) = 0;\\
\delta\theta_x: &\quad a_{22}\theta_y' + a_{25}(v_0' + \theta_x) = 0; \qquad \delta\theta_y: \quad a_{33}\theta_x' + a_{34}(u_0' + \theta_y) = 0.
\end{aligned} \tag{11a–d}$$

The coefficients $a_{ij} = a_{ji}$ and b_i appearing in these equations as well as in the forthcoming ones denote stiffness and reduced mass terms, respectively. Their expressions are displayed in Appendix A. Equations (9) and (11) reveal that in the context of the above considered ply angle configuration, in addition to the already mentioned elastic couplings, the transverse shear is also coupled with lagwise bending, and lagwise (chordwise) transverse shear is coupled with flapwise bending. Moreover, the Coriolis acceleration, where the pertinent terms are underscored by a dotted line, induces a supplementary coupling

between the flapping and lagging bendings. Separately from the above mentioned couplings, the extension–twist one is induced by the same ply angle configuration. This type of coupling is important and implemented as such, e.g., in helicopter blades and tilt rotor aircraft.

Corresponding to the extension–twist motion the governing system is

$$\delta w_0: \quad a_{11}w_0'' + a_{17}\phi'' - b_1\ddot{w}_0 = 0,$$

$$\delta\phi: \quad -a_{66}\phi'''' + a_{17}w_0'' + a_{77}\phi'' - (b_4 + b_5)\ddot{\phi} + (b_{10} + b_{18})\ddot{\phi}'' + (b_4 + b_5)\Omega^2\phi = 0, \tag{12a, b}$$

whereas the associated boundary conditions are

$$\text{At } z = 0, \qquad w_0 = \phi = \phi' = 0 \tag{13a–c}$$

and, at $z = L$,

$$\delta w_0: \quad a_{11}w_0' + a_{17}\phi' = 0,$$

$$\delta\phi: \quad -a_{66}\phi'''' + a_{17}w_0' + a_{77}\phi' + (b_{10} + b_{18})\ddot{\phi}' = 0,$$

$$\delta\phi': \quad a_{66}\phi'' = 0. \tag{14a–c}$$

One should remark that in the system of equations associated with the extension–twist coupling, equations (12), the Coriolis effect is not involved. Moreover, Ω^2 involves only the twist equation. This implies that in the absence of the twist-extension coupling (i.e., of $a_{17} = 0$), the two equations become decoupled and, as such, the extension motion becomes independent on Ω^2.

5. SPECIAL CASES

Two special cases which involve bending–bending–transverse shear coupling are reported herein. In this context, Case (i) corresponds to axisymmetric shearable thin-walled beams whose constituent materials feature orthotropic properties, the principal axes of orthotropy being parallel to the geometrical axes. In this case, the coupling stiffness quantities $a_{43} = a_{52} = 0$, and as a result of the postulated axisymmetry of the construction,

$$a_{22} = a_{33} \equiv A, \qquad a_{44} = a_{55} \equiv B, \qquad b_4 + b_{14} = b_5 + b_{15} \equiv C. \tag{15a–c}$$

In terms of complex displacement variables defined as

$$U = u_0 + \mathrm{i}v_0, \qquad \Theta = \theta_y + \mathrm{i}\theta_x, \qquad (\mathrm{i} = \sqrt{-1}), \tag{16a, b}$$

the governing equations reduce to

$$BU'' + B\Theta' - b_1\ddot{U} - 2\mathrm{i}b_1\Omega\dot{U} + b_1U\Omega^2 = 0, \qquad A\Theta'' - BU' - B\Theta - C\ddot{\Theta} = 0, \tag{17a, b}$$

while the homogeneous boundary conditions at $z = 0, L$ read:

$$B(U' + \Theta) = 0 \quad \text{or} \quad U = 0; \qquad A\Theta' = 0 \quad \text{or} \quad U' = 0. \tag{18a, b}$$

It is readily seen that the stiffness quantity B associated with the transverse shear effect couples the two governing equations. Solutions of the eigenvalue problem based on this complex representation can be found e.g., in references [11–13]. Case (ii), involves the non-shear deformable case. Elimination from equations (9) and (11) of the quantities $a_{44}(u_0'' + \theta_y')$ and $a_{55}(v_0'' + \theta_x')$, followed by consideration of equation (3) stating

the absence of transverse shear, results in the governing equations of motion:

$$\delta u_0: \quad a_{22}u_0'''' + b_1\ddot{u}_0 - (b_5 + b_{15})\ddot{u}_0'' - \underline{2}\underline{b_1}\underline{\Omega}\underline{\dot{v}_0} - b_1 u_0\Omega^2 = 0,$$

$$\delta v_0: \quad a_{33}v_0'''' + b_1\ddot{v}_0 - (b_4 + b_{14})\ddot{v}_0'' + \underline{2}\underline{b_1}\underline{\Omega}\underline{\dot{u}_0} - b_1 v_0\Omega^2 = 0, \tag{19a, b}$$

and of the boundary conditions which have to be prescribed. Their homogeneous counterpart is

$$a_{22}u_0''' - (b_5 + b_{15})\ddot{u}_0' = 0 \quad \text{or} \quad u_0 = 0; \quad a_{33}v_0''' - (b_4 + b_{14})\ddot{v}_0' = 0 \quad \text{or} \quad v_0 = 0,$$

$$a_{22}u_0'' = 0 \quad \text{or} \quad u_0' = 0; \quad a_{33}v_0'' = 0 \quad \text{or} \quad v_0' = 0. \tag{20a–d}$$

It should be remarked that the governing equations of shearable thin-walled beams, (equations (9)), and their non-shear deformable counterparts, equations (19), feature the same order (eight) and as such, four boundary conditions have to be prescribed, in both cases, at each end $z = 0, L$ of the beam. These equations are formally similar to the ones obtained in the context of a solid beam (e.g., see references [6] and [7]). Equations (19) reveal that in this special case, the coupling arises only via the Coriolis acceleration effect. In their absence both equations would be decoupled. As a result, upon defining the complex displacement variable $U(\equiv u_0 + \mathrm{i}v_0)$, the governing equation system becomes

$$AU'''' + b_1\ddot{U} - B\ddot{U}'' + 2\mathrm{i}b_1\Omega\dot{U} = 0, \tag{21}$$

whereas the homogeneous boundary conditions reduce to

$$AU''' - B\ddot{U}' = 0 \quad \text{or} \quad U = 0, \quad AU'' = 0 \quad \text{or} \quad U' = 0. \tag{22}$$

In this case, in order to study the associated eigenvalue problem a modal analysis can be implemented. The problem was approached in this manner in a number of papers (e.g., in references [6–9]).

6. THE EIGENVALUE PROBLEM OF GYROSCOPIC SYSTEMS: NUMERICAL ILLUSTRATIONS

As previously mentioned, there are special cases when the modal analysis can be applied to solve the eigenproblem associated with the bending–bending–transverse shear coupled motion. However, for the case described by equations (9)–(11), the modal analysis fails to provide a solution to the associated eigenproblem. In contrast to this and to this goal, the displacement functions are represented in the form

$$(u_0(z, t), \quad v_0(z; t), \quad \theta_x(z; t), \quad \theta_y(z; t)) = (u(z), v(z), \hat{\theta}(z), \hat{\hat{\theta}}(z))\, \mathrm{e}^{\lambda t}, \tag{23}$$

where λ stands for the complex frequency while u, v, $\hat{\theta}$ and $\hat{\hat{\theta}}$ denote the amplitudes of u_0, v_0, θ_x and θ_y, respectively. The amplitude functions are represented as

$$u = \sum_{j=1}^{n} a_j u_j(z), \; v = \sum_{j=1}^{n} b_j v_j(z), \; \hat{\theta} = \sum_{j=1}^{n} c_j \hat{\varphi}(z), \; \hat{\hat{\theta}} = \sum_{j=1}^{n} d_j \hat{\hat{\varphi}}(z), \tag{24a–d}$$

where $u_j(z), \ldots, \hat{\hat{\varphi}}(z)$ are trial functions which have to fulfill the kinematic boundary conditions. Employment of representations (23) and (24) in the variational integral, (6), carrying out the indicated variations and the required integrations, yields the equations expressed in matrix form as

$$\mathbf{D}\delta\mathbf{B} = 0, \tag{25}$$

where $\mathbf{D}$ $(\equiv \mathbf{A}_0\lambda^2 + \mathbf{A}_1\lambda + \mathbf{A}_2)$ is a polynomial in λ with matrix coefficients where $\mathbf{A}_0$ and

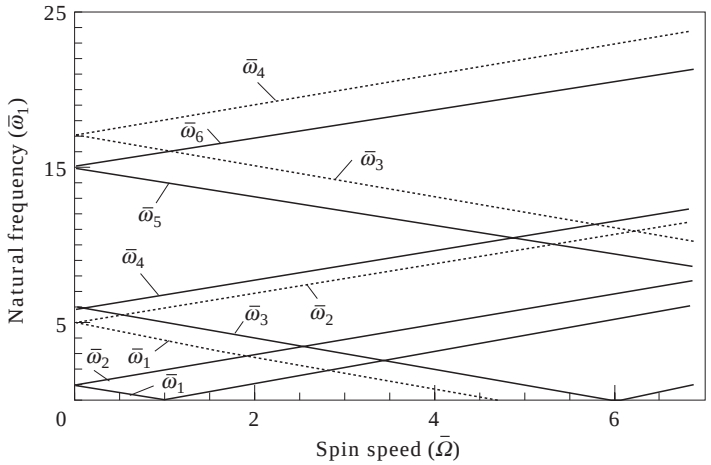

Figure 2. Rotating frequency-spin rate interaction for a beam of $R = 1$, and $\theta = 0^\circ$ and 90°: ——, $\theta = 0^\circ$; · · · ·, $\theta = 90^\circ$.

$\mathbf{A}_2$ are real matrices, $\mathbf{A}_1$ is real and skew-symmetric while $\delta\mathbf{B} \equiv (\delta a_j, \delta b_j, \delta c_j, \delta d_j)^{\mathrm{T}}$. From equation (25), the non-triviality condition for $\delta\mathbf{B}$ requires the fulfillment of

$$\det\left(\mathbf{A}_0\lambda^2 + \mathbf{A}_1\lambda + \mathbf{A}_2\right]) = 0. \tag{26}$$

For a technique enabling one to solve the eigenvalue problem associated with equation (26) see references [22] and [23] and for a discussion of this method adapted to Matlab see reference [24]. According to the method in references [22] and [23] the eigenvalues of the original eigenvalue problem, equation (26), are the same as those of the associated standard eigenvalue problem

$$[\mathbf{Z} - \lambda\mathbf{I}] = 0, \tag{27}$$

where the $4n \times 4n$ state matrix $[\mathbf{Z}]$ is given by

$$\mathbf{Z} = \left[\begin{array}{c|c} \mathbf{0} & \mathbf{I} \\ \hline -\mathbf{A}_o^{-1}\mathbf{A}_2 & -\mathbf{A}_o^{-1}\mathbf{A}_1 \end{array}\right] \tag{28}$$

while $\mathbf{I}$ is the unitary matrix of order $4n$. If $\mathbf{Z}$ is real, the eigenvalues occur in $2n$ pure imaginary complex conjugate pairs $\lambda_r = \pm \mathrm{i}\omega_r$ $(r = \overline{1, 2n})$ where ω_r are the *rotating* (whirling) frequencies. The values of $\bar{\Omega}$ rendering zero-valued eigenvalues correspond to the divergence instability. In Figures 2–7 graphical representations of the dependence of natural rotating frequencies upon the spin rate are displayed. All the results are recorded in terms of the spin speed Ω and natural frequencies ω_i normalized by the fundamental natural frequency $\hat{\omega}$ of the non-rotating beam counterpart, this yielding the normalized spin rate speed $\bar{\Omega}(\equiv \Omega/\hat{\omega})$ and natural rotating frequencies $\bar{\omega}_i(\equiv \omega_i/\hat{\omega})$. Herein $\hat{\omega} = 265{\cdot}5$ rad/s corresponds to a square cross-section beam with clamped–free boundary conditions whose material is characterized by $\theta = 0^\circ$. In addition, all the numerical illustrations are carried out for the case of a box-beam of rectangular cross-section of fixed dimensions $c = 4$ in, $L = 40$ in, $h = 0{\cdot}4$ in, whose constituent material is graphite–epoxy. For its elastic characteristics see e.g., reference [5]). In Figure 2 the dependence $\bar{\omega}_i$, $(i = 1, 2, 3)$ versus $\bar{\Omega}$ for a square cross-section beam $R(\equiv b/c) = 1$, whose material is

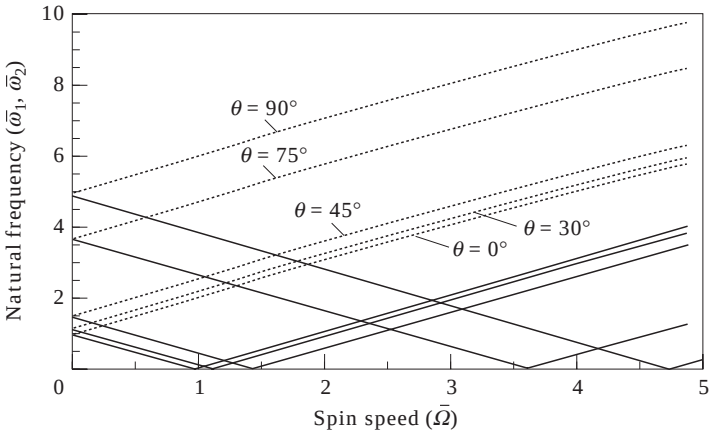

Figure 3. The influence of the ply angle on rotating frequency–spin rate interaction for a beam of $R = 1$: ——, $\bar{\omega}_1$; · · · ·, $\bar{\omega}_2$.

characterized by the ply angles $\theta = 0^\circ$ and 90°, is displayed. For the present case ($R = 1$) and for the non-rotating beam ($\bar{\Omega} = 0$) the flapping and lagging frequencies, in each mode coincide. With the increase of $\bar{\Omega}$, a bifurcation of natural frequencies is experienced, where the upper and lower branches correspond to the backward whirl and forward whirl, respectively. The minimum spin rate at which the rotating natural frequency becomes zero-valued, is called the critical spinning speed, denoted as $\bar{\Omega}_{cr}$. Figure 2 reveals that the beam characterized by the ply angle $\theta = 90^\circ$ features a considerably larger $\bar{\Omega}_{cr}$ than its beam counterpart characterized by $\theta = 0^\circ$.

In Figure 3, the effects of the ply angle on the frequency-spin rate interaction of a square cross-section beam are displayed. The results reveal that for each ply-angle there is a specific critical spinning speed and that, for this case, the minimum and maximum ones occur for $\theta = 0^\circ$ and $\theta = 90^\circ$, respectively.

In Figure 4, the influence of three different combinations of boundary conditions on the frequency-spin interaction is graphically represented. The results reveal that the minimum $\bar{\Omega}_{cr}$ occurs for the clamped–free beam, the maximum one for the clamped–clamped beam, whereas the intermediate one occurs for simply supported at both end beams.

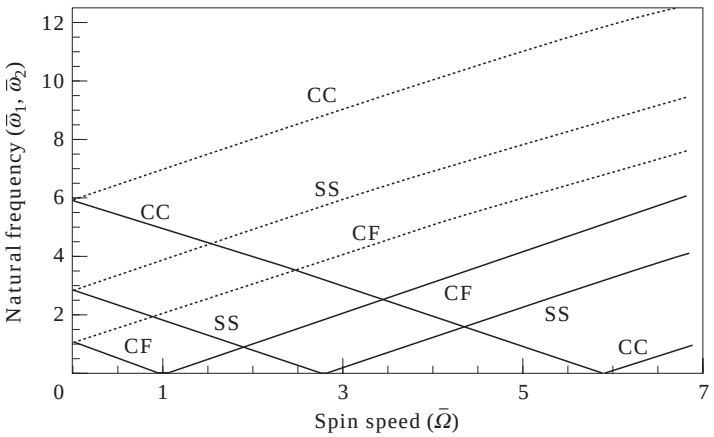

Figure 4. The influence of boundary conditions on rotating frequency–spin rate interaction for a beam of $R = 1$, $\theta = 0^\circ$: ——, $\bar{\omega}_1$; · · · ·, $\bar{\omega}_2$.

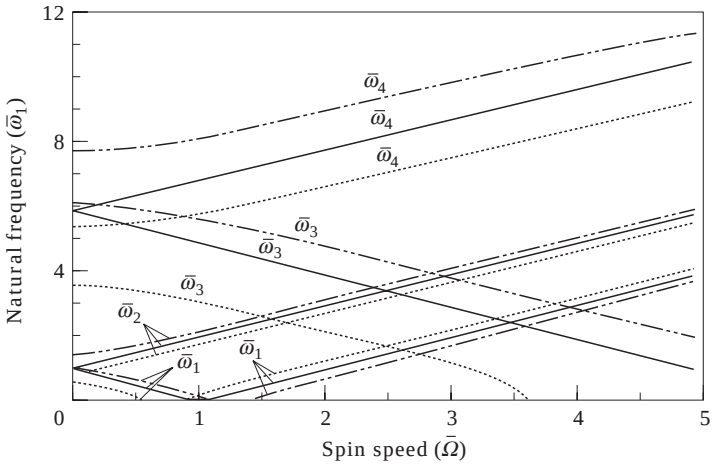

Figure 5. The influence of the non-symmetry of the beam cross-section measured in terms of $R(R = 1, 0{\cdot}5$ and $1{\cdot}5)$ on rotating frequency–spin rate interaction, $\theta = 0^\circ$: ——, $R = 1$; · · · ·, $R = 0{\cdot}5$; —— · · · ——, $R = 1{\cdot}5$.

Figures 5 through 7 reveal the effects played by the non-symmetry of the beam cross-section, measured in terms of the parameter $R(\equiv b/c)$ on the frequency-spin rate interaction. The results emerging from these plots reveal that for a beam characterized by $R \neq 1$, the non-rotating bending frequencies in flapping and lagging do not coincide. In addition, for this case, instead of a critical spinning speed, there is a whole domain of critical spinning speeds for which the dynamic system becomes unstable. Moreover, Figure 5 reveals that the domain of instability can be shifted toward larger spin speeds by tailoring the structure. However, as it becomes evident from this graph, this shift of the instability domain towards larger spin rates is paid for by an enlargement of the domain of instability. Figure 6 reveals that the shift of the domain of instability towards larger spin speeds can result also via the combination of different boundary conditions. At this point, the same remark related to the enlargement of the domain of instability which is accompanied by this shift, is in order. The results of Figure 5 also reveal that for the beam cross-sections characterized by $R > 1$, the domain of instability is shifted toward

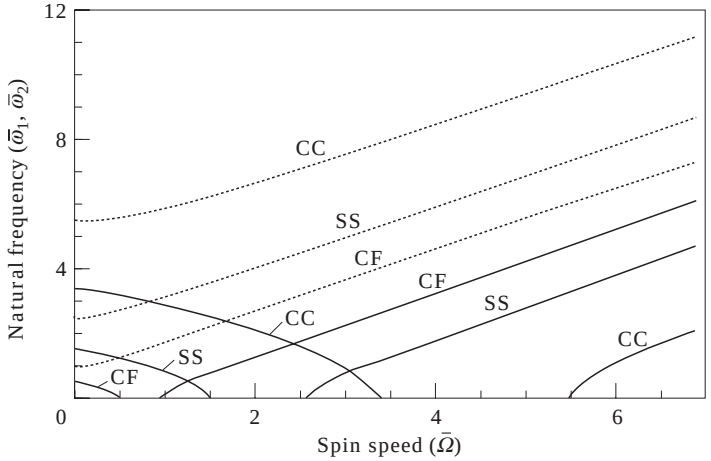

Figure 6. The influence of boundary conditions on rotating frequency–spin rate interaction of a beam characterized by $R = 0{\cdot}5$ and $\theta = 0^\circ$: ——, $\bar{\omega}_1$; · · · ·, $\bar{\omega}_2$.

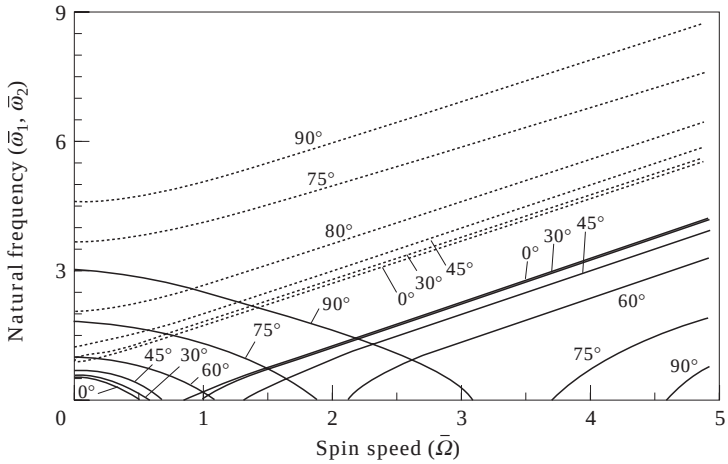

Figure 7. The influence of ply angle on rotating frequency–spin rate interaction for a beam of $R = 0{\cdot}5$: ——, $\bar{\omega}_1$; · · · ·, $\bar{\omega}_2$.

larger spin rates but the extent of the *domain* of instability is similar to that one occurring for beams featuring $R < 1$. From Figure 5 it becomes apparent that the increase of the ply angle is accompanied by the enlargement of the instability domains and their shift towards larger spin rates.

It should be remarked that the result related to the divergent critical condition obtained in reference [27] for a non-shear deformable spinning *solid* beam has the counterpart in the case of thin-walled beams. In order to obtain it, starting with the equations (19), considered in conjunction with the representations (23), upon enforcing the condition $\lambda = 0$ (condition of divergence) and applying a Rayleigh quotient procedure to the resulting equations, one finds

$$\hat{\Omega}^2_{cr} = \int_0^L a_{22}(\bar{u}_0'')^2 \, \mathrm{d}z \Big/ \int_0^L b_1 \bar{u}_0^2 \, \mathrm{d}z \quad \text{and} \quad \hat{\bar{\Omega}}^2_{cr} = \int_0^L a_{33}(\bar{v}_0'')^2 \, \mathrm{d}z \Big/ \int_0^L b_1 \bar{v}_0^2 \, \mathrm{d}z. \tag{29}$$

In equations (27), $\hat{\Omega}^2_{cr}$ and $\hat{\bar{\Omega}}^2_{cr}$ denote the critical speen speeds in divergence associated with lagging and flapping motions, respectively. For an axisymmetric cross-section beam the two critical velocities are identical. Otherwise, the lowest of the two is the most critical one and should be taken into consideration. In equations (29), $\bar{u}_0(z)$ and $\bar{v}_0(z)$ are modal shape functions corresponding to the lagging and flapping motions, respectively. In the case of clamped–free boundary conditions, $\bar{u}_0(z)$ has to fulfill the boundary conditions

$$\bar{u}_0 = \bar{u}_0' = 0 \text{ at } z = 0. \tag{30}$$

Similar boundary conditions obtained by replacing $\bar{u}_0 \rightarrow \bar{v}_0$ have to be implemented when the flapping motion is considered.

It should be remarked that in the case of the *unloaded* spinning thin walled beams, the instability can occur only by divergence. In the case of loaded spinning beams, the instability can occur also by flutter. Details on these issues can be found in references [25–29].

7. SPINNING THIN WALLED BEAMS SUBJECTED TO A LONGITUDINAL COMPRESSIVE DEAD FORCE

In the present section the stability of a spinning thin walled beam subjected at its free end to a longitudinal compressive dead force will be investigated. For the sake of

simplicity, the case of an axisymmetric non-shearable beam clamped at $z = 0$ and free at $z = L$ is considered.

Based on equations (19) and (20), using the denotations displayed in equation (15) and the results of reference [30], the governing equations are

$$Au_0'''' + Pu_0'' + b_1\ddot{u}_0 - 2b_1\Omega\dot{v}_0 - b_1u_0\Omega^2 - C\ddot{u}_0'' = 0,$$

$$Av_0'''' + Pv_0'' + b_1\ddot{u}_0 + 2b_1\Omega\dot{u}_0 - b_1v_0\Omega^2 - C\ddot{v}_0'' = 0, \tag{31a, b}$$

while the boundary conditions are

$$z = 0: \qquad u_0 = 0, \qquad u_0' = 0, \qquad v_0 = 0, \qquad v_0' = 0; \tag{32a–d}$$

$$z = L: \qquad Au_0''' + Pu_0' - C\ddot{u}_0' = 0, \qquad Au_0'' = 0;$$

$$Av_0''' + Pv_0' - C\ddot{v}_0' = 0, \qquad Av_0'' = 0. \tag{32e–h}$$

In these equations P denotes the end load positive in compression. Expressing equations (31) and (32) in terms of the complex displacement U defined by equation (16a) and letting

$$U(z, t) = \phi(z)\, e^{i\omega t}, \tag{33}$$

where $\phi(z)$ and ω are complex valued quantities, one obtains the equation

$$A\phi'''' + P\phi'' - b_1(\omega^2 + \Omega^2)\phi - 2b_1\Omega\omega\phi + C\omega^2\phi'' = 0, \tag{34}$$

and the boundary conditions:

$$z = 0: \qquad \phi = 0, \qquad \phi' = 0; \tag{35a, b}$$

$$z = L: \qquad A\phi''' + P\phi' + C\omega^2\phi' = 0, \qquad A\phi'' = 0. \tag{35c, d}$$

Multiplying equation (34) by the complex conjugate of ϕ, namely $\overline{\phi}$, integrating the resulting equation over the beam span length and using the boundary conditions (35), one obtains

$$K\omega^2 + G\omega + Q = 0, \tag{36}$$

where

$$K = b_1 \int_0^L \phi\overline{\phi}\, dz + C \int_0^L \phi'\overline{\phi}'\, dz - C(\overline{\phi}(L)\phi'(L) + \phi(L)\overline{\phi}'(L)),$$

$$G = 2b_1\Omega \int_0^L \phi\overline{\phi}\, dz,$$

$$Q = b_1\Omega^2 \int_0^L \phi\overline{\phi}\, dz + P \int_0^L \phi'\overline{\phi}'\, dz - A \int_0^L \phi''\overline{\phi}''\, dz - \tfrac{1}{2}P(\overline{\phi}(L)\phi'(L) + \phi(L)\overline{\phi}(L)). \tag{37a–c}$$

In equation (37) the three terms in succession are associated with the kinetic energy, conservative gyroscopic energy and potential energy of the system, respectively. From equation (36), the condition for the neutral flutter instability requires ω to be a purely real valued quantity, which implies the fulfillment of the condition $G^2 - 4KQ = 0$. This condition represents a statement of coalescence of two eigenfrequencies.

This condition provides the compressive load yielding the flutter of the snapping thin-walled beam:

$$P_{flutter} = S_1/S_2, \tag{38}$$

where

$$S_1 = b_1 A \int_0^L \phi\overline{\phi}\,\mathrm{d}z \int_0^L \phi''\overline{\phi}''\,\mathrm{d}z - Cb_1\Omega^2 \int_0^L \phi'\overline{\phi}'\,\mathrm{d}z \int_0^L \phi\overline{\phi}\,\mathrm{d}z$$

$$+ CA \int_0^L \phi\overline{\phi}\,\mathrm{d}z \int_0^L \phi''\overline{\phi}''\,\mathrm{d}z + Cb_1\Omega^2(\overline{\phi}(L)\phi'(L) + \phi(L)\overline{\phi}'(L)) \int_0^L \phi\overline{\phi}\,\mathrm{d}z$$

$$- CA(\overline{\phi}(L)\phi'(L) + \phi(L)\overline{\phi}'(L)) \int_0^L \phi''\overline{\phi}''\,\mathrm{d}z,$$

$$S_2 = b_1 \int_0^L \phi\overline{\phi}\,\mathrm{d}z \int_0^L \phi'\overline{\phi}'\,\mathrm{d}z - \tfrac{1}{2}b_1(\overline{\phi}(L)\phi'(L) + \phi(L)\overline{\phi}'(L)) \int_0^L \phi\overline{\phi}\,\mathrm{d}z$$

$$+ C \int_0^L \phi'\overline{\phi}'\,\mathrm{d}z \int_0^L \phi'\overline{\phi}'\,\mathrm{d}z - C(\overline{\phi}(L)\phi'(L) + \phi(L)\overline{\phi}'(L)) \int_0^L \phi'\overline{\phi}'\,\mathrm{d}z$$

$$+ C[\overline{\phi}(L)\phi'(L) + \phi(L)\overline{\phi}'(L)]^2. \tag{39a, b}$$

In the absence of rotatory inertia terms, i.e., when $C = 0$, the flutter condition becomes

$$P_{flutter} = A \int_0^L \phi''\overline{\phi}''\,\mathrm{d}z \Big/ \left(\int_0^L \phi'\overline{\phi}'\,\mathrm{d}z - \tfrac{1}{2}(\overline{\phi}(L)\phi'(L) + \phi(L)\overline{\phi}(L)) \right). \tag{40}$$

In view of equations (38) and (39), one should conclude that when the rotatory inertia effect is incorporated (i.e., $C \neq 0$), the flutter condition includes also Ω.

However, when its effect is discarded, according to equation (40), $P_{flutter}$ is independent of Ω. A similar result has been obtained also in reference [27].

From equation (36), one also obtains the condition of the occurrence of the divergence instability. This is given by

$$Q = 0. \tag{41}$$

Having in view that in the case of the divergence instability the eigenvalues and eigenfunctions are real valued quantities, one obtains

$$P_{div} = \left(A \int_0^L (\phi'')^2\,\mathrm{d}z - b_1\Omega^2 \int_0^L \phi^2\,\mathrm{d}z \right) \Big/ \left(\int_0^L (\phi')^2\,\mathrm{d}z - \phi(L)\phi'(L) \right), \tag{42a}$$

or

$$\Omega_{div}^2 = \left(A \int_0^L (\phi'')^2\,\mathrm{d}z - P \int_0^L \phi^2\,\mathrm{d}z + P\phi(L)\phi'(L) \right) \Big/ b_1 \int_0^L (\phi^2\,\mathrm{d}z), \tag{42b}$$

Equation (42a) shows that P_{div} diminishes with the increase in Ω^2, a conclusion revealed also numerically in reference [10].

Finally, in the absence of the compressive end load from equation (41) one obtains

$$\Omega_{div}^2 = A \int_0^L (\phi'')^2 \, dz \Big/ b_1 \int_0^L \phi^2 \, dz, \tag{43}$$

a result which coincides with that given by equation (29).

Associated with the problem considered in this section, by using the mathematical methodologies developed in references [25–29], a more comprehensive approach, resulting in the possibility of incorporating a number of additional effects such as transverse shear and non-symmetry of the cross-section can be pursued.

Needless to say, also in the case considered herein, the influence of ply angle orientation on flutter and divergence instability conditions can be analyzed and pertinent results on stability enhancement stability can be obtained.

8. THE CASE OF THE EXTENSION–TWIST COUPLING

In the case of extension–twist motion, due to the absence of the Coriolis effect, a standard eigenvalue problem is reached. As a result, for each mode number, a single branch of the natural frequency–spinning speed dependence is obtained.

In Figure 8 the first non-dimensionalized eigenfrequency $\bar{\omega}_1(\equiv \omega_1/\hat{\omega})$ versus the non-dimensional speen speed $\bar{\Omega}(\equiv \Omega/\hat{\omega})$ for various ply angles is depicted. For this case, $\hat{\omega} = 1937{\cdot}8$ rad/s is the first coupled extension–twist eigenfrequency determined for a non-spinning beam characterized by $\theta = 0^\circ$, $R = 1$ and clamped–free boundary conditions. The results in this plot reveal that the frequency $\bar{\omega}_1$ is highly dependent on $\bar{\Omega}$ and, consequently, in this case the twist is dominant. From this plot it is also seen that at the

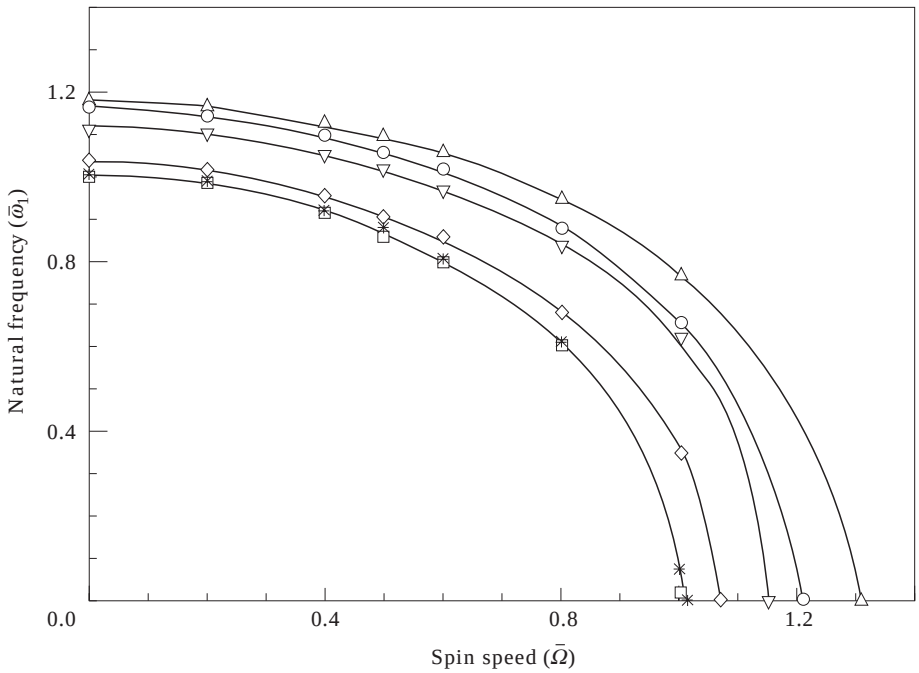

Figure 8. Fundamental eigenfrequency $\bar{\omega}_1$ versus speen speed for different ply angles for a beam of $R = 1$, featuring extensional-twist cross-coupling: —×—, 0°; —○—, 30°; —△—, 45°; —▽—, 60°; —◇—, 75°; —□—, 90°.

ply angles $\theta = 0^\circ$, 90° and $\theta = 45^\circ$, minimum and maximum critical speen speeds are reached, respectively.

However, corresponding to specific values of the ply angle for which the extension–twist cross-coupling, a_{17}, is very weak, but the extensional stiffness a_{11} is very strong, sensitivity of the variation of eigenfrequencies with that of $\bar{\Omega}$ would be almost immaterial. In such a case the motion is extension-dominant. Conversely, for the cases when the extension–twist cross-coupling is weak while the twist and warping stiffnesses a_{77} and a_{66}, respectively, are strong, the motion will be strongly influenced by $\bar{\Omega}$. In this case the motion is twist–dominant.

9. CONCLUSIONS

An analytical study devoted to the mathematical modelling of spinning thin walled beams has been presented. Based on the derived equations, an assessment of the influence of a number of non-classical effects on their vibrational and instability behavior has been accomplished. Among others, the results reveal that structural tailoring can be successfully employed to enhance their behavior by increasing the spinning speed and shifting the domain of divergence instability towards larger spin rates.

The results provided in this paper should be useful for a better design of spinning structures used in advanced technology.

ACKNOWLEDGMENTS

This work was supported in part by the Korea Science and Engineering Foundation (KOSEF 951-1002-030-2), support which is gratefully acknowledged by O. Song. Technical discussions with Professor R. H. Plaut from Virginia Polytechnic Institute and State University are appreciated.

REFERENCES

1. H. F. Bauer 1980 *Journal of Sound and Vibration* **72**, 177–189. Vibration of a rotating uniform beam. Part I. Orientation in the axis of rotation.
2. P. L. Hetherington, R. F. Kraus and M. S. Darlow 1990 *Journal of the American Helicopter Society* **35**, 23–28. Demonstrations of a supercritical composite helicopter power transmission shaft.
3. C. W. Bert and C. D. Kim 1995 *Journal of Vibration and Acoustics* **117**, 17–21. Whirling of composite material driveshafts including bending–twisting coupling and transverse shear deformation.
4. L. W. Rehfield and A. R. Atilgan 1989 Proceedings of the First USSR–US Symposium on Mechanics of Composite Materials, May, 187–196. Toward understanding the tailoring mechanisms for thin-walled composite tubular beams.
5. O. Song and L. Librescu 1993 *Journal of Sound and Vibration* **167**, 129–147. Free vibration of anisotropic composite thin-walled beams of closed cross-section contour.
6. P. W. Likins, F. J. Barbera and V. Baddeley 1973 *AIAA Journal* **11**, 1251–1258. Mathematical modeling of spinning elastic bodies for modal analysis.
7. C. P. Filipich, M. J. Maurizi and M. B. Rosales 1987 *Journal of Sound and Vibration* **116**, 475–482. Free vibrations of a spinning uniform beam with ends elastically restrained against rotation.
8. C. P. Filipich, M. J. Maurizi and M. B. Rosales 1989 *Journal of Sound and Vibration* **129**, 350–355. A note on the free vibration of a spinning beam.
9. C. W. Lee, R. Katz, A. G. Ulsoy and R. A. Scott 1988 *Journal of Sound and Vibration* **122**, 119–130. Modal analysis of a distributed parameter rotating shaft.
10. M. L. Chen and Y. S. Liao 1991 *Journal of Sound and Vibration* **147**, 497–513. Vibrations of pretwisted spinning beams under axial compressive loads with elastic constraints.

11. T. Saito and M. Endo 1986 *Bulletin of JSME* **29**, 1239–1245. Vibration analysis of rotating cylindrical shells based on the Timoshenko beam theory.
12. R. P. S. Han and J. W. Z. Zu 1992 *Journal of Sound and Vibration* **156**, 1–16. Modal analysis of rotating shafts. A body fixed axis formulation approach.
13. J. W.-Z. Zu and R. P. S. Han 1992 *Transactions of the ASME*, *Journal of Applied Mechanics* **59**, 197–204. Natural frequencies and normal modes of a spinning Timoshenko beam with general boundary conditions.
14. C. L. Liao and Y. H. Dang 1992 *Computers and Structures* **45**, 715–731. Structural characteristics of spinning pretwisted orthotropic beams.
15. A. Zohar and J. Aboudi 1973 *International Journal of Mechanical Sciences* **15**, 269–278. The free vibrations of a thin circular finite rotating cylinder.
16. S. C. Huang and W. Soedel 1988 *Journal of the Acoustical Society of America* **84**, 275–285. On the forced vibration of simply supported rotating cylindrical shells.
17. O. Rand and Y. Stavsky 1991 *International Journal of Solids and Structures* **28**, 831–843. Free vibrations of spinning composite cylindrical shells.
18. C. D. Kim and C. W. Bert 1993 *Composites Engineering* **3**, 633–643. Critical speed analysis of laminated composite hollow drive shaft.
19. C. W. Bert and C. D. Kim 1995 *Dynamic and Stability of Systems* **10**, 125–147. Dynamic instability of composite-material drive shaft subject to fluctuating torque and/or rotational speed.
20. L. Librescu and O. Song, *Composites Engineering* [Special Issue: *Use of Composites in Rotorcraft and Smart Structures*] **2**, 497–512. On the static aeroelastic tailoring of composite aircraft swept wings modeled as thin-walled beam structures.
21. E. C. Smith and I. Chopra 1991 *Journal of the American Helicopter Society* **36**. Formulation and evaluation of an analytical model for composite box beams.
22. L. Meirovitch 1979 *AIAA Journal* **21**, 1337–1342. A new method of solution of the eigenvalue problem for gyroscopic systems.
23. L. Meirovitch 1980 *Computational Methods in Structural Dynamics*. Alphen an den Rijn, The Netherlands: Sijthoff and Nordhoff.
24. D. J. Inman and M. J. Atalla 1995 *SAVIAC*, *SVM*-13 *Shock and Vibration Computer Programs* (Editors Walter and Barbara Pilkey). Calculating modal data and time responses.
25. K. Huseyin and R. H. Plaut 1974–1975 *Journal of Structural Mechanics* **3**, 163–177. Transverse vibrations and stability of systems with gyroscopic forces.
26. K. Huseyin and R. H. Plaut 1975 *Dynamics of Rotors*, *IUTAM Symposium*, *Lyngby*, *Denmark*, *August* 12–16, 1974, 182–205. Berlin: Springer-Verlag; Divergence and flutter boundaries of systems under combined conservative and gyroscopic forces.
27. R. C. Shieh 1971 *International Journal of Non-Linear Mechanics* **5**, 495–509. Energy and variational principles for generalized (gyroscopic) conservative problems.
28. R. C. Shieh 1982 *Journal of Applied Mechanics* **49**, 191–196. Some principles of elastic shaft stability including variational principles.
29. C. W. Lee and J. S. Yun 1996 *Journal of Sound and Vibration* **192**, 439–452. Dynamic analysis of flexible rotors subjected to torque and force.
30. K. Bhaskar and L. Librescu 1995 *International Journal of Engineering Science* **33**, 1331–1344. A geometrically nonlinear theory for laminated anisotropic thin-walled beams.

APPENDIX A: EXPRESSIONS OF STIFFNESS $a_{ij}(\equiv a_{ji})$ AND REDUCED MASS TERMS b_i

$$a_{11} = \oint K_{11}\,\mathrm{d}s, \quad \text{extensional stiffness (lb);}$$

$$a_{17} = \oint K_{13}\,\mathrm{d}s, \quad \text{extension–twist coupling stiffness (1b in);}$$

$$a_{22} = \oint [K_{11}x^2 + 2xK_{14}\,\mathrm{d}y/\mathrm{d}s + K_{44}(\mathrm{d}y/\mathrm{d}s)(\mathrm{d}y/\mathrm{d}s)]\,\mathrm{d}s, \qquad \text{bending (lag) stiffness (lb in}^2\text{);}$$

$$a_{25} = \oint (xK_{12}\,\mathrm{d}y/\mathrm{d}s + K_{24}(\mathrm{d}y/\mathrm{d}s)(\mathrm{d}y/\mathrm{d}s))\,\mathrm{d}s,$$

bending (lag)–transverse shear coupling stiffness (lb in);

$$a_{33} = \oint (K_{11}y^2 - 2yK_{14}\,\mathrm{d}x/\mathrm{d}s + K_{44}(\mathrm{d}x/\mathrm{d}s)(\mathrm{d}x/\mathrm{d}s))\,\mathrm{d}s, \qquad \text{bending (flap) stiffness [lb in}^2\text{];}$$

$$a_{34} = \oint (K_{12}\,y\mathrm{d}x/\mathrm{d}y + K_{14}(\mathrm{d}x/\mathrm{d}s)(\mathrm{d}x/\mathrm{d}s))\,\mathrm{d}s,$$

bending (flap)–transverse shear coupling stiffness (lb in);

$$a_{44} = \oint (K_{22}(\mathrm{d}x/\mathrm{d}s)(\mathrm{d}x/\mathrm{d}s) + A_{44}(\mathrm{d}y/\mathrm{d}s)(\mathrm{d}y/\mathrm{d}s))\,\mathrm{d}s,$$

transverse shear stiffness in x direction (lb);

$$a_{55} = \oint (K_{22}(\mathrm{d}y/\mathrm{d}s)(\mathrm{d}y/\mathrm{d}s) + A_{44}(\mathrm{d}x/\mathrm{d}s)(\mathrm{d}x/\mathrm{d}s))\,\mathrm{d}s,$$

transverse shear stiffness in y direction (lb);

$$a_{66} = \oint [K_{11}F_\omega^2 + 2K_{14}F_\omega a + K_{44}a^2]\,\mathrm{d}s, \qquad \text{warping stiffness (lb in}^4\text{);}$$

$$a_{77} = \oint [2(A_c/\beta)K_{23}]\,\mathrm{d}s, \qquad \text{torsional stiffness (lb in}^2\text{).}$$

In addition,

$$(b_1, b_4, b_5, b_{10}) = \oint m_0(1, y^2, x^2, F_\omega^2)\,\mathrm{d}s, \qquad (b_{14}, b_{15}, b_{18}) = \oint m_2\left(\frac{\mathrm{d}x}{\mathrm{d}s}\right)^2, \left(\frac{\mathrm{d}y}{\mathrm{d}s}\right)^2, a^2\Big)\,\mathrm{d}s;$$

where

$$(m_0, m_2) = \sum_{k=1}^{N} \int_{h_{(k-1)}}^{h_{(k)}} \rho_{(k)}(1, n^2)\,\mathrm{d}n.$$

In the above expressions K_{ij} are defined as

$$K_{11} = A_{22} - A_{12}^2/A_{11}, \qquad K_{12} = A_{26} - A_{12}A_{16}/A_{11} = K_{21},$$
$$K_{44} = D_{22} - B_{12}^2/A_{11}, \qquad K_{13} = 2K_{12}A_c/\beta,$$

$$K_{22} = A_{66} - A_{16}^2/A_{11}, \qquad K_{23} = 2K_{22}A_c/\beta, \qquad K_{24} = B_{26} - A_{16}B_{12}/A_{11} = K_{42}.$$

In these expressions A_{ij}, B_{ij} and C_{ij} denote the local stretching and bending stiffness components, respectively.